THERMAL ISSUES AT THE SSC

Raj P Ranganathan and Bui V Dao

Accelerator Systems Division

Superconducting Super Collider

2550 Beckleymeade Avenue

Dallas, TX 75237

(Presented at the Fourth Annual Thermal & Fluids Analysis Workshop, Cleveland, OH, August 17-21, 1992. Sponsored by the Thermal & Fluids Analysis Branch, NASA Lewis Research Center. Also published in the proceedings of the meeting.)

1.0 ABSTRACT

A variety of heat transfer problems arise in the design of the Superconducting Super Collider (SSC). One class of problems is to minimize heat leak from the ambient to the SSC rings, since the rings contain superconducting magnets maintained at a temperature of 4 K. Another arises from the need to dump the beam of protrons (traveling around the SSC rings) on to absorbers during an abort of the collider. Yet another category of problems is the cooling of equipment to dissipate the heat generated during operation. An overview of these problems and sample heat transfer results are given in this paper.

2.0 INTRODUCTION

Figure 1 gives a birds-eye-view of the Dallas/Fort Worth area and the SSC main underground tunnel. The 87 km circumference tunnel will contain two main rings of magnets and other components [1].

Figure 2 shows a cross-section of the main tunnel. Two counter-rotating beams of protons will travel inside the two main rings at nearly the speed of light. Collision of these beams under controlled conditions is expected to yield new sub-atomic particles that will unravel mysteries of the origins of the universe.

The purpose of this paper is to give an overview of some of the heat transfer problems that arise in the design of the SSC and present sample heat transfer results.

3.0 CLASSIFICATION OF HEAT TRANSFER PROBLEMS

The heat transfer problems encountered at SSC can be classified (based upon their applications) into the following categories:

3.1 Heat Leak

Minimization of heat leak from the ambient to the components of the SSC main and High Energy Booster rings (that span a total route length of 185 km). The interior of these components is maintained at 4 K, since they contain superconducting magnets. Therefore, minimizing heat leak can lower refrigeration costs. References [2] through [6] are a small sample of the vast amount research reported on this subject.

3.2 Beam Absorption

Absorption of the beam of protons by depositing the beam on to absorbers may be necessary during commisioning of the SSC rings or during an abort of the rings [7]. Under accident conditions the beam could be deposited on to the superconducting magnets itself [8]. In addition, during beam deposition on to target materials (for physics experiments), a similar heat transfer problem arises.

3.3 Cooling of Equipment

Different equipment generate heat during their operation. The heat must be carried away by an optimum cooling system that does not jeopardise the various operational specifications of the equipment.

4.0 HEAT LEAK INTO THE SPOOL PIECE

4.1 Description

Figure 3 shows one of the components of the SSC rings, the spool piece [1]. At the spool piece, cryogen (helium and nitrogen) lines enter and leave the rings. The spool piece also contains safety valves for the cryogen tubing and in addition performs numerous other functions.

The spool piece is also characterized by a complex geometry with numerous heat flow paths between the ambient and the 4 K interior. Therefore, accurately predicting heat leak into the spool piece is a challenging task.

At steady state, the flow of heat into the spool piece from the ambient will be carried away by cryogen flowing at three temperature levels, namely 80 K, 20 K and 4 K. The cryogen at 80 K is liquid nitrogen, at 20 K it is gaseous helium and at 4 K it is liquid helium. The maximum temperature rise in the 4 K cryogen line is fractions of a degree kelvin, while in the 20 and 80 K cryogen lines, it is about 8 K.

4.2 Model Assumptions and Solution Details

In order to estimate the heat leak from the spool piece, the following simplifying assumptions were made:

1) heat flow through conduction paths is steady and one-dimensional,

2) residual gas conduction across the vacuum spaces is accounted for,

3) thermal radiation across the vacuum spaces is taken into account,

4) thermo-physical properties are a function of temperature,

5) natural convection of the cryogen in valves is neglected.

Numerous other secondary assumptions were made for the convenience of the analysis but are omitted here in the interests of brevity.

The conduction calculations were made using integral tables, while the effects of thermal radiation was accounted for by

means of simple calculations based on more detailed and accurate calculations [9]. The effect of residual gas conduction was based on empirical expressions [10].

4.3 Results

Table 1 summarizes the heat leak results for one of the many spool piece variants at SSC. Of greatest concern is the heat leak at the 4 K level since refrigeration costs are higher at lower temperatures. Table 1 shows that the total heat leak into the 4 K cryogen is nearly 9 W with the copper instrumentation leads accounting for more than 5 W.

A detailed thermal resistance analysis [6,9], possibly using available software in the market, may improve the accuracy of the heat leak estimates. Research has shown that natural convection flows of the stagnant cryogen in the valves may contribute to heat leak [11,12]. This assumption may have to be relaxed. Efforts are also underway to obtain measurements of the heat leak. More details of the calculations reported here can be obtained by contacting the principal author of this paper.

5.0 BEAM ABSORBER

5.1 Description

Figure 4 shows a schematic of an iron absorber for the SSC linear accelerator (LINAC). The beam of protons has an elliptic cross-section, with 2 mm and 20 mm axes, and is incident on the front surface of the absorber. Within the absorber, the energy of the protons is converted into internal energy of the absorber through a sequence of physics processes, the theory about which is available elsewhere [13].

The calculation of the energy deposition rates is accomplished by the most recent version of the MARS software [14]. As the beam penetrates the absorber, it assumes a cone shape and the energy deposition is correspondingly over a three-dimensional conical region within the absorber. The apex of the cone is at the point of incidence on the front surface of the absorber and the axis of the cone coincides with the axis of the beam. At the axis of the beam, the energy deposition rate is 4 orders of magnitude greater than at a radial distance of 1 cm. Thus high thermal stresses can be expected at the axis.

Thus, the problem here is to determine the duration of beam deposition that is permissible without exceeding the peak temperature and stress limit for a given absorber material.

5.2 Model Assumptions and Solution Details

The assumptions made to determine the peak temperature and stresses in the absorber were:

1) heat conduction is transient and three-dimensional,

2) heat generation rates are a function of t, x, y and z,

3) thermo-physical properties are temperature dependent.

The problem was solved using ANSYS and computer times of the order of 1 day were required on the HP-730 workstation for each calculation.

5.3 Results

Figure 5 shows the peak temperature and stresses versus time for an iron absorber core for two different beam deposition scenarios. The scenarios were determined based on physics considerations [15]. Peak temperature and von-mises stress limits of 500 C and 200 MPa were specified, keeping in view the melting point of iron which is approximately 1500 C [16] and the yield point of iron under tension which is approximately 200 to 500 MPa [17].

The operational scenario (solid lines on Figure 5), involves a 1 GeV (giga electron volts) beam of protons impinging on the absorber in a series of pulses. Each pulse has a 7 micro-second duration and the corresponding current over that duration is 25 mA. The frequency of the pulses is 10 Hz. Further, the pulses arrive at the absorber in batches of 7, spanning 0.7 seconds. Each batch of 7 pulses is separated by a 6.3 second time interval from neighbouring batches. Thus, there are 7 pulses every 7 seconds.

For the operational scenario, the beam can be deposited on the absorber for 16 hrs without exceeding the above limits. Therefore, for the given scenarios, an iron sbsorber should be sufficient. Details of this work will be published shortly.

6.0 LIQUID COOLED RF-CAVITY TUNER

6.1 Description

Figures 6a and 6b show typical low energy booster radio frequency (rf) cavity. The function of the cavity is to accelerate the proton beam to higher energy levels [1].

Figure 7 shows a sectional view of an rf-cavity tuner. There are 4 ferrite disks of 25 mm thickness each, separated by 5 mm spaces. (Note, Figures 6a and 6b show 5 ferrites, while Figure 7 considers a configuration with 4 ferrites.) Coolant flows through the spaces between the ferrites to dissipate the heat generated in the ferrites, and in the walls of the tuner housing during the operation of the rf-cavity. Note the location of the coolant inlets and exits on Figures 6a through 7. The coolant inlets are diametrically opposite the exits.

The problem is to design an optimum cooling system that prevents high temperatures in the ferrites and the coolant. If the peak temperature in the ferrites approaches its curie temperature (125 C) then its magnetic properties are affected. Similarly, the peak temperature in the coolant should not approach its boiling point. In the case of one of the coolants considered here, the Galden Heat Transfer Liquid, the boiling point was 110 C. Details of this work are available elsewhere [18].

6.2 Model Assumptions and Solution Details

The following assumptions were made in the analysis [18]:

1) the heat transfer in the coolant and the flow field are steady, incompressible, three-dimensional and turbulent,

2) natural convection is included,

3) heat conduction in the ferrites is three-dimensional,

4) heat generation in the ferrites, coolant and copper is included,

5) the thermo-physical properties of the coolant and ferrite are constant,

6) geometric complexities neglected.

Due to reflective symmetry, two symmetry planes were identified normal to the axial and azimuthal directions, each of which bi-

sected the tuner to two mirror-image halves [18]. Thus the computational domain encompased only one-fourth of the tuner shown on Figures 6a and 6b.

The problem was solved using the PHOENICS computational fluid dynamics (CFD) package. About 25,000 cells were used and computer times of several days was needed on the HP-730 workstation [18]. No comparisons of calculations with measurements have been made. When such data become available in the future, comparisons will be made. No grid dependence studies were made due to the enormous computer resources involved.

6.3 Results

Figure 8 illustrates a typical flow field on the axial-direction symmetry plane. Clearly the coolant prefers the path of least resistance along the annular passage between the ferrites and the tuner housing. Reducing the annular gap can induce the coolant to flow into the interior where cooling is needed.

The isotherms (also on the axial-direction plane of symmetry) of Figure 9 show a recirculation region. The peak ferrite temperatures were located there.

The isobars (near the side wall of the housing) of Figure 10 show that the bulk of the pressure drop in the fluid occurs near the exits.

In summary, the peak ferrite and coolant temperatures were sensitive to: coolant flow rate, coolant inlet temperature, inlet and exit areas, number of inlets and exits and the annular gap [18]. The calculations also indicated that natural convection effects played an important role in lowering the local temperatures in the coolant and ferrite[18,19].

The sensitivity studies helped influence the design of the cooling system.

7.0 SOLID COOLED RF-CAVITY TUNER

7.1 Description

A solid-cooled version of the rf-cavity described above was evaluated. Disks of Beryllium Oxide (BeO) or Aluminum Nitride (alnide) were placed in the coolant spaces between the ferrites

(Figure 7) as shown on Figure 11 [20]. Five ferrite disks are used in this case (Figure 11) versus four in the earlier liquid cooled case. Good thermal contact between the BeO (or alnide) disks and the ferrite disks was facilitated by having a film of goop (a glue) between them. The glue also helped reduce thermal stresses in the ferrites and BeO (or alnide). Details of this work can be found in Reference [20].

Due to the high thermal conductivity of the BeO (286 W/mC) or the alnide (170 W/mC) compared to that of the ferrite (5.5 W/mC), the heat generated in the ferrites was transported to the housing walls by the BeO and alnide. At the housing walls the heat is removed by flowing a coolant such as water within tubes brazed on the outside of the housing. Thus, the BeO and alnide disks serve as paths of low thermal resistance that carry the heat away from the ferrites [20].

The problem involves heat conduction through complex geometries, with dissimilar solids bonded together. Therefore, the peak temperatures and stresses in the solids have to be determined.

It is important that the peak temperatures in the ferrites not approach its curie temperature (125 C) and the peak stresses in the ferrites, BeO and alnide yield a safety factor of at least 3 compared with the strengths of the respective materials. Table 2 shows the relevant strengths of the different materials.

7.2 Model Assumptions and Solution Details

The following assumptions were made:

1) transient, three-dimensional heat conduction,

2) heat generation rates vary with time and radius,

3) properties are constant.

The problem was solved using ANSYS and cpu times of several hrs were required on the HP-730 workstation for each case.

7.3 Results

Figures 12a and 12b show the computational domain from two different views. Notice the ferrites, BeO, copper housing walls and copper ribs outside the housing. The complexity of the geometry is evident.

Table 2 shows steady state temperature and stress results obtained for a typical case. Use of BeO gave the lowest peak temperature and stresses for all the cases considered. Use of alnides came second while the non-use of either BeO or alnide had the highest peak temperatures and stresses. In summary, solid cooling the tuner using BeO was found to be feasible from a thermal and stress perspective. Details are available elsewhere [20].

8.0 REFERENCES

1) "Site-Specific Conceptual Design of the Superconducting Super Collider," Material prepared by the staff of the SSC Laboratory, Editors: J. R. Sanford and D. M. Mathews, Superconducting Super Collider Laboratory Report SSCL-SR-1056, July 1990.

2) McAshan, M., Thirumaleshwar, M., Abramovich, S., Ganni, V. and Scheidemantle, A., "84 K Nitrogen system for the SSC," published in Supercollider 4, Proceedings of the IISSC, New Orleans, February, 1992.

3) Nicol, N. H., "SSC 50 mm collider dipole cryostat single tube support post conceptual design and analysis," SSC report number SSCL-N-765, July 9, 1991.

4) Carcagno, R. H., McAshan, M. S., and Schiesser, W. E., " A helium venting model for an SSC half cell," published in Supercollider 3, Proceedings of the IISSC, Atlanta, 1991.

5) Boroski, W. N., Nicol, T. H., and Schoo, C. J., "Design of the multilayer insulation system for the Superconducting Super Collider 50 mm dipole cryostat," published in Supercollider 3, Proceedings of the IISSC, Atlanta, 1991.

6) Franks, D. E. and Pletzer, R. K., "The effect of vacuum gas pressures and species on internal heat leak in the SSCL magnet design," published in Supercollider 4, Proceedings of the IISSC, New Orleans, February, 1992.

7) Hauviller, C., Schonbacher, H., van Steenbergen, A., "Beam dump absorber for the 400 x 400 GeV p-p superconducting large storage rings (Isr)," CERN report no. CERN-ISR-GE/79-4, 1979.

8) VanGinnekin, A., "Distribution of heat due to beam loss in energy doubler saver type superconducting magnets," Fermi Lab report number TM-685, 1976.

9) Pletzer, R., "Results of revised analysis of 50 mm dipole magnets with and without 4 K and 20 K MLI blanket," SSC memo number 925830HM, March 23, 1992.

10) Barron, R. F., Cryogenic Systems, Oxford University Press, New York, 1985.

11) Timmerhaus, K. D., and Gu Y., "Theoretical analysis of thermal acoustic oscillation systems," presented at the XVIII th Int. Congress of Refrigeration, Montreal, Quebec, Canada, August 10-17, 1991.

12) Kuzmina, A. G., "Thermoacoustic oscillations in cryostats: new results," Cryogenics, vol. 32, no. 1, pp. 11-19, 1992.

13) Patterson, H. W. and Thomas, R. H., "Accelerator Health Physics," Academic Press, Inc., New York, 1973.

14) Mokhov, N. V., "The MARS10 Code System: Inclusive Simulation of Hadronic and Electromagnetic Cascades and Muon Transport," Fermi National Accelerator Laboratory Report FN-509, March, 1989.

15) McGill, J., Bull, J., Shailey, R., and Wang, F., physicists at Superconducting Super Collider Laboratories, 1992.

16) Lide, D. R., "Handbook of Chemistry and Physics," 71 st Edition, CRC Press, Boston, 1990-1991.

17) "Handbook of Mathematical, Scientific, and Engineering Formulas, Tables, Functions, Graphs, Transforms," Staff of Research and Education Association, Dr. M. Fogiel, Director, Research and Education Association, New Jersey, 1984.

18) Ranganathan, R. P., "Tuner thermal analysis," presented at the rf Workshop, TRIUMPF, Vancouver, B.C., Canada, January 21-24, 1992.

19) Campbell, B., "SSC LEB Cavity Mechanical Design Considerations," presented at the rf Workshop, TRIUMPF, Vancouver, B.C., Canada, October 25-26, 1990.

20) Ranganathan, R. P., "Solid Cooled Tuner," presented at the rf Workshop, SSC Labs, Dallas, Texas, June 25, 1992.

Table 1: ASST SPR spool piece heat load summary

	HEAT LEAK PATHS	LOCATION IN SPOOL PIECE (mW) 4 K	20 K	80 K
1	Floating Support	15	320	2103
2	Instrumentation Tuving (Lead End)	89	0	0
3	Cool-Down Valve Tubing	0	0	2849
4	4 K Relief Tubing & Cryogen Conv.	0	0	891
5	Correction Element Power Lead ASSY	1930	0	0
6	20 K Relief Tubing & Cryogen Conv.	0	109	804
7	Quench Line	28	95	0
8	Recooler Valve	165	0	556
	Stainless Steel Housing	[88]	[0]	[551]
	G-10 Housing	[6]	[0]	[45]
	UHMW Plug-In Stem	[71]	[0]	[0]
9	Recooler Valve Pressure Tubing	88	537	5042
10	Fixed Support	15	320	2103
11	Deflection Stops	24	0	0
12	Instrumentation Tubing (Middle)	174	0	0
13	Vacuum Barrier (With Cu Straps)	78	1573	10775
14	Instrumentation Tubing (Return End)	106	0	0
15	Beam Tube Pump Port	55	0	581
16	Radiation Between Shields	1	192	8441
17	Residual Gas Conduction	33	60	6
18	Interconnect Regions	0	42	38
19	99.99 % Cu Instrumentation Wires	5222	0	0
	J1 (8 22-AWG; 7 28-AWG)	[757]	[0]	[0]
	J2 (12 14-AWG)	[4067]	[0]	[0]
	JSPR (60 30-AWG)	[56]	[0]	[0]
	JRE1 (60 30-AWG)	[342]	[0]	[0]
20	Manganin Instrumentation Wires	7	1	2
	J3 (40 32-AWG)	[4]	[0]	[0]
	JVAC (36 32-AWG)	[3]	[1]	[2]
21	BPM Cables	120	0	0
22	Safety Leads	2	0	0
23	Opening Near Vacuum Barrier	201	0	0
	TOTAL CALCULATED ASST HEAD LOAD	8353	3249	34191
24	Dynamic Heat Load	462	0	0
	TOTAL CALCULATED ASST HEAT LOAD	8715	3249	34191
	TOTAL BUDGETED COLLIDER HEAT LOAD	2288	11321	57710

Greg Cruse, John Nguyen, Raj Ranganathan, Andy Scheidemantle, Ken Schiffman
02/28/92

Table 2: Thermal/stress results of solid cooled low energy booster rf-cavity tuner

1	No. of Alnide Disks	0	2	0
2	No. of BeO Disks	0	0	2
	BEO			
1	Max T (° C)	-	-	59
2	Max Tension (MPa)	-	-	8
3	Tensile Strength (MPa)	-	-	151
4	Safety Factor	-	-	18.9
	ALNIDE			
1	Max T (° C)	-	63	-
2	Max Tension (MPa)	-	32	-
3	Flexural Strength (MPa)	-	46	-
4	Safety Factor	-	1.4	-
	FERRITE			
1	Max T (° C)	85	66	62
2	Curie T (° C)	125	125	125
3	Max Tension (MPa)	26	15	14
4	Tensile Strength (MPa)	39	39	39
5	Safety Factor	1.5	2.6	2.8
	GOOP			
1	Max T (° C)	83	66	61
2	Max Operating T (° C)	150	150	150
3	Max Shear (MPa)	<< 1	<< 1	<< 1
4	Lap Shear Strength (MPa)	7	7	7
5	Safety Factor	>> 7	>> 7	>> 7
	COPPER			
1	Max Stress (MPa)	25	25	24
2	Yield Strength (MPa)	69	69	69
3	Safety Factor	2.8	2.8	2.9

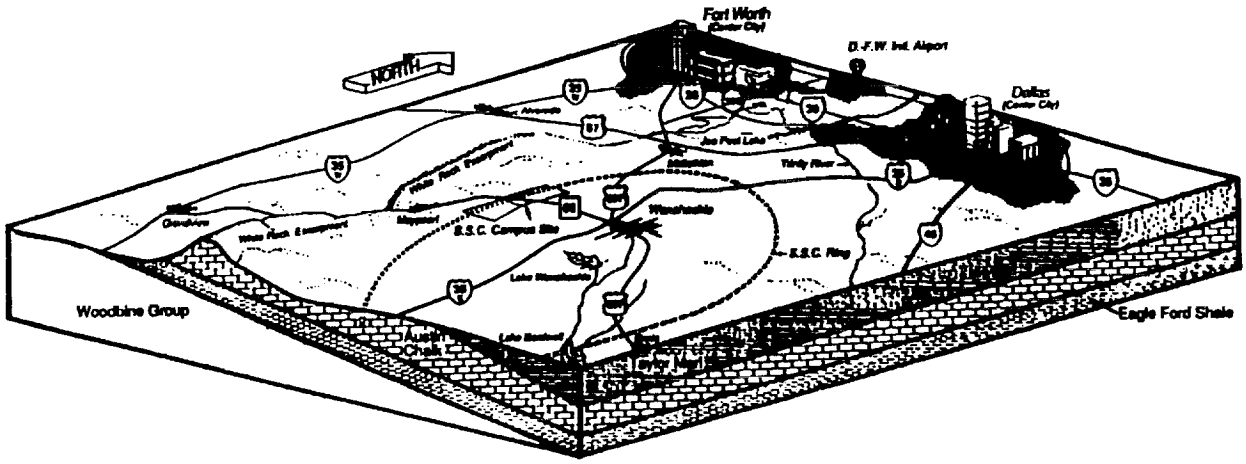

Figure 1: Topographic and geologic profile along ring circumference [1].

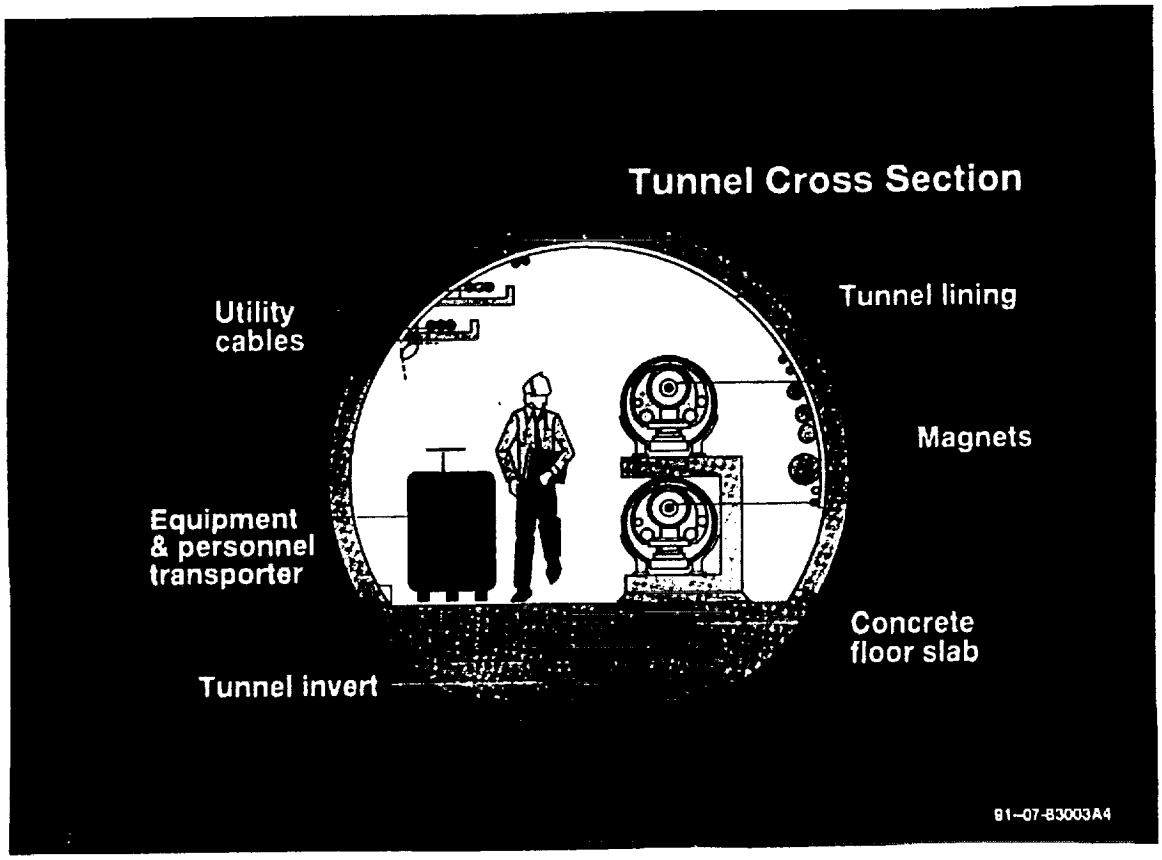

Figure 2: Cross section of the main SSC tunnel

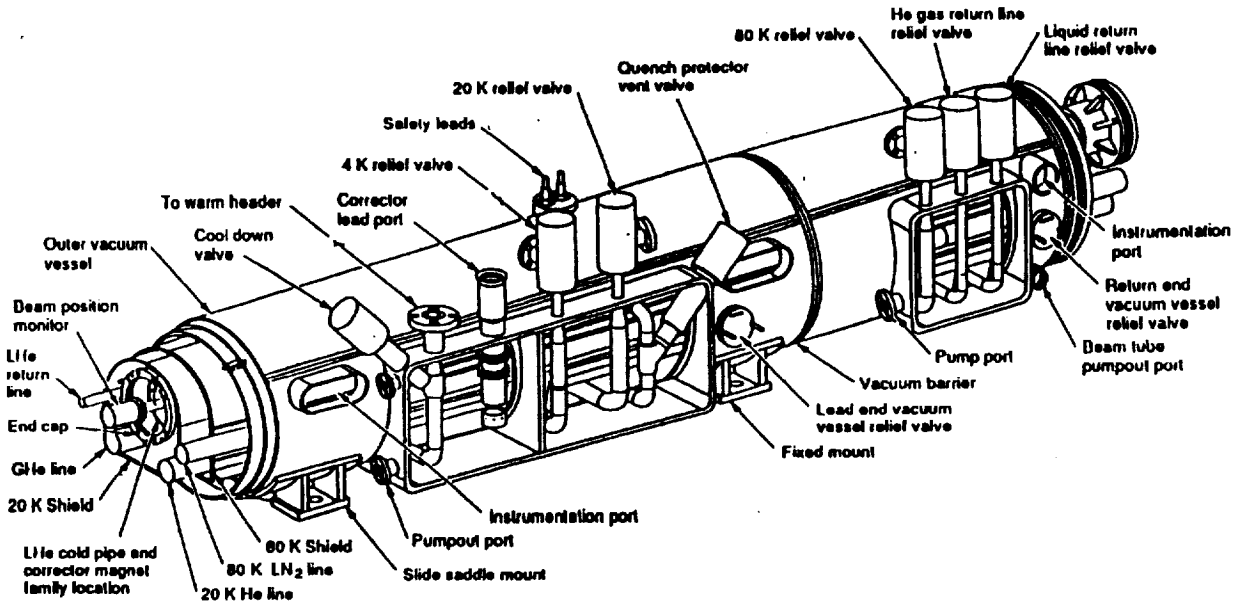

Figure 3: Standard spool piece

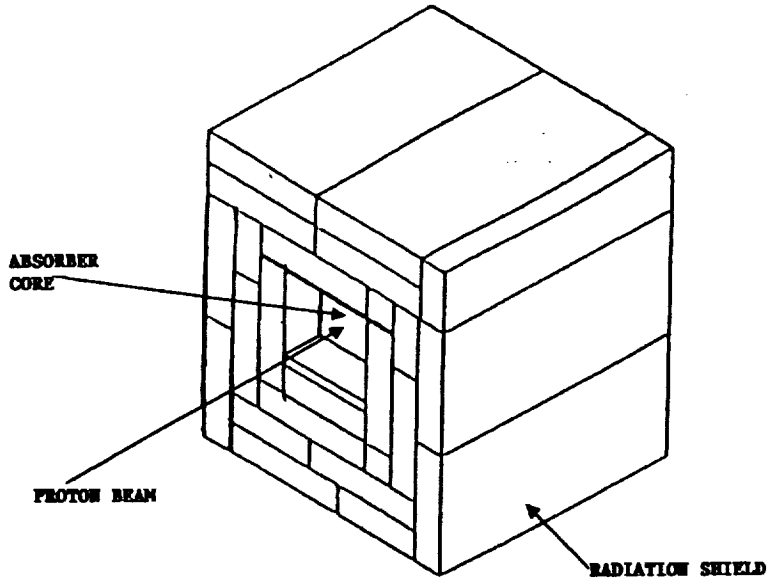

Figure 4: Schematic of a beam absorber

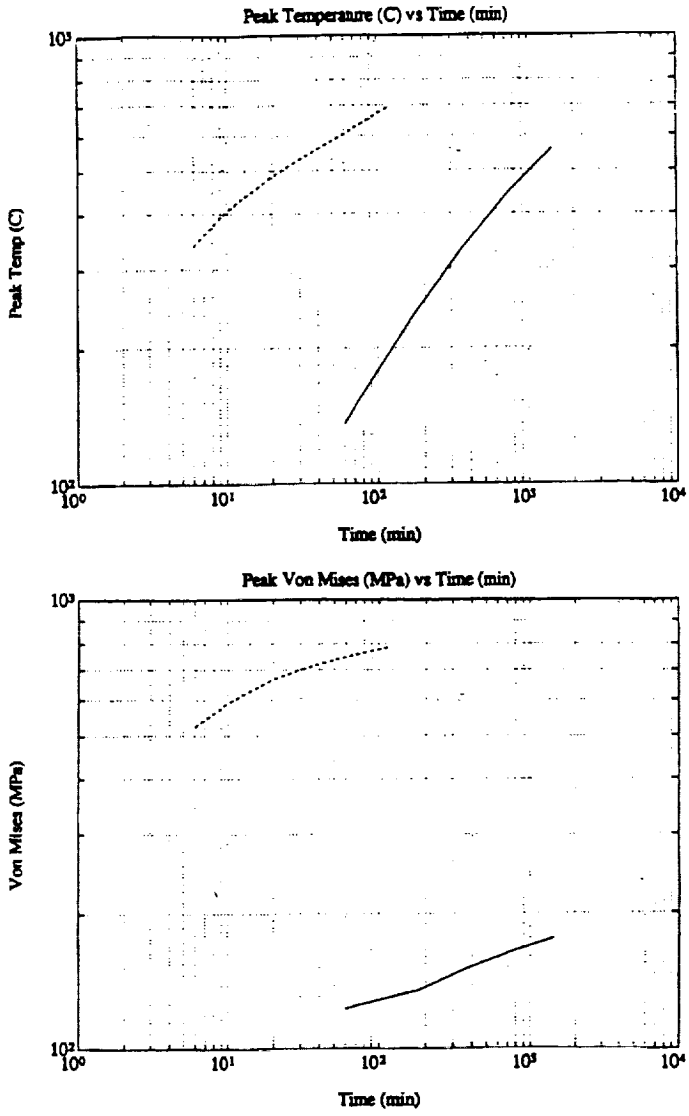

— 1 GeV, 25 mA, 7 mic-s pulse @ 10 Hz, 7 pulses / 7 s

- - 1 GeV, 50 mA, 35 mic-s pulse @ 10 Hz, continuous

Figure 5: Peak temperatures and stresses in the LINAC beam absorber

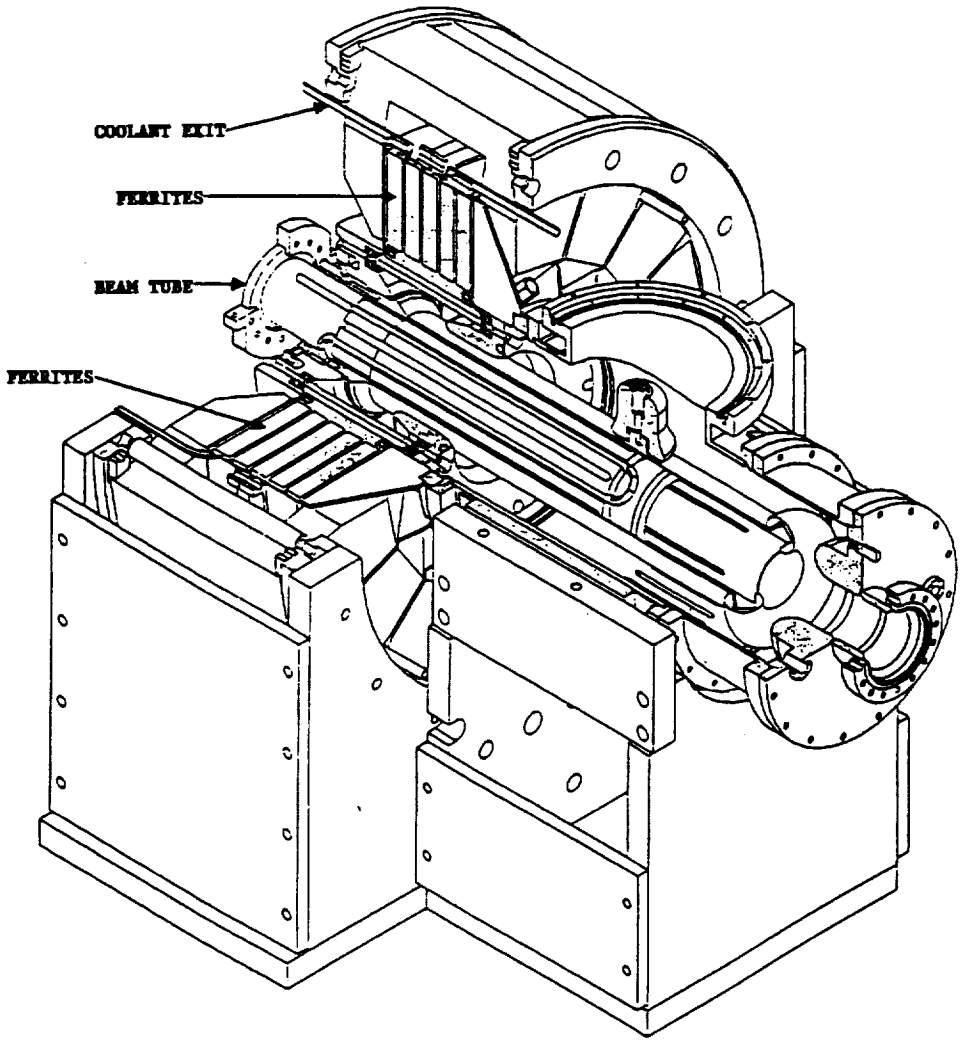

Figure 6a: Representative low energy booster rf-cavity

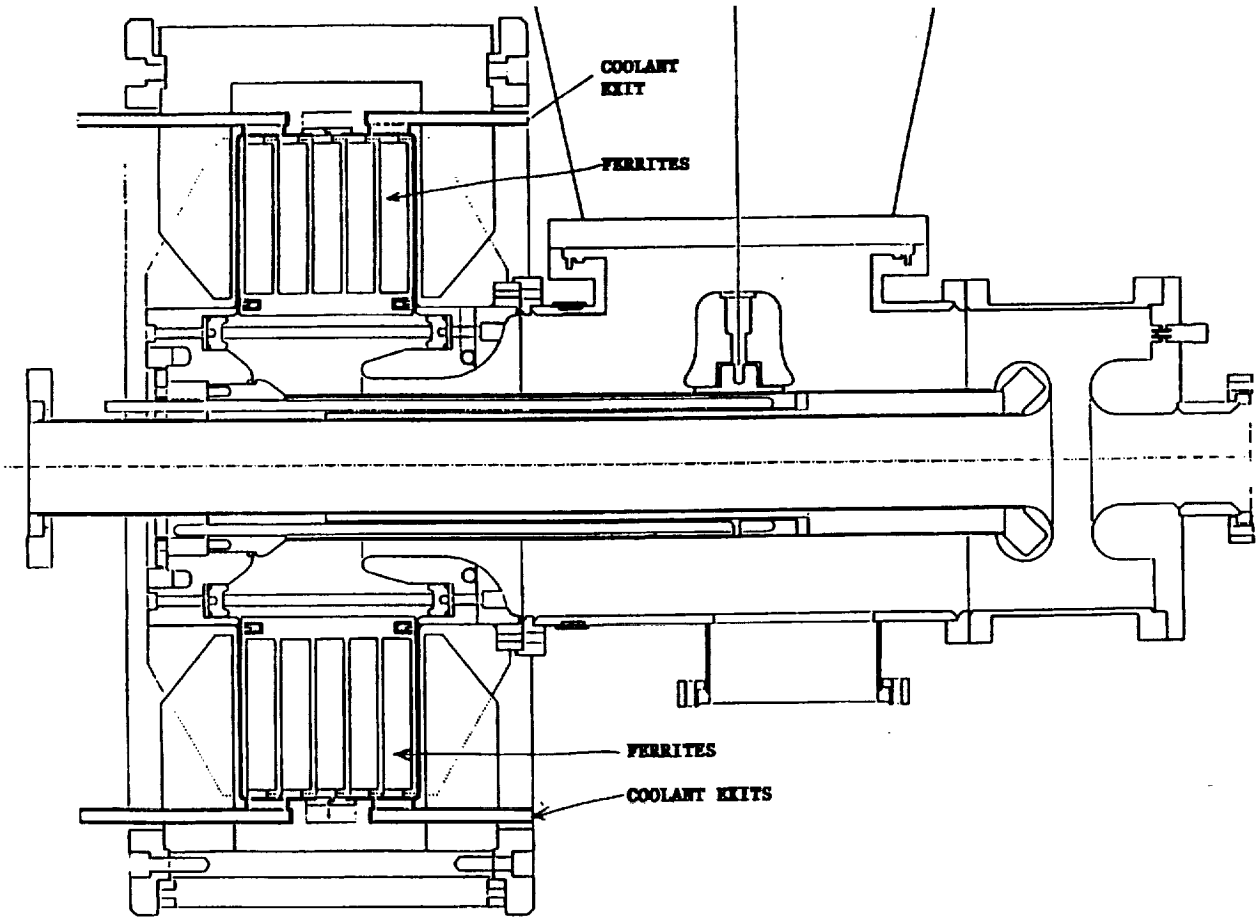

Figure 6b: Representative low energy booster rf-cavity – sectional view

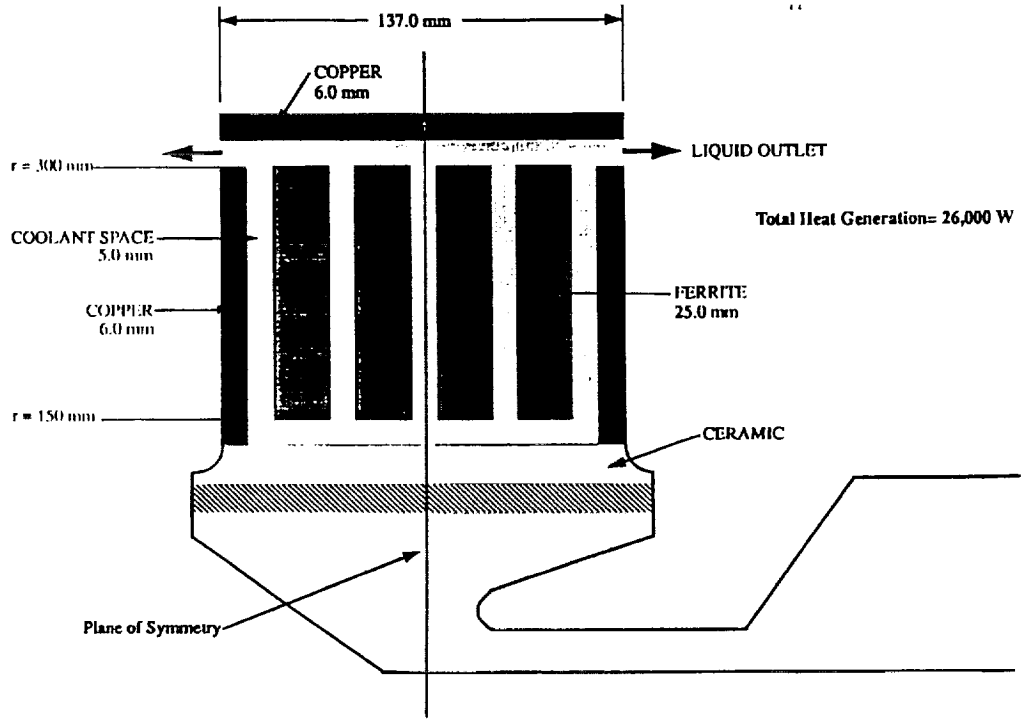

Figure 7: Sectional view of liquid-cooled low energy booster rf cavity tuner

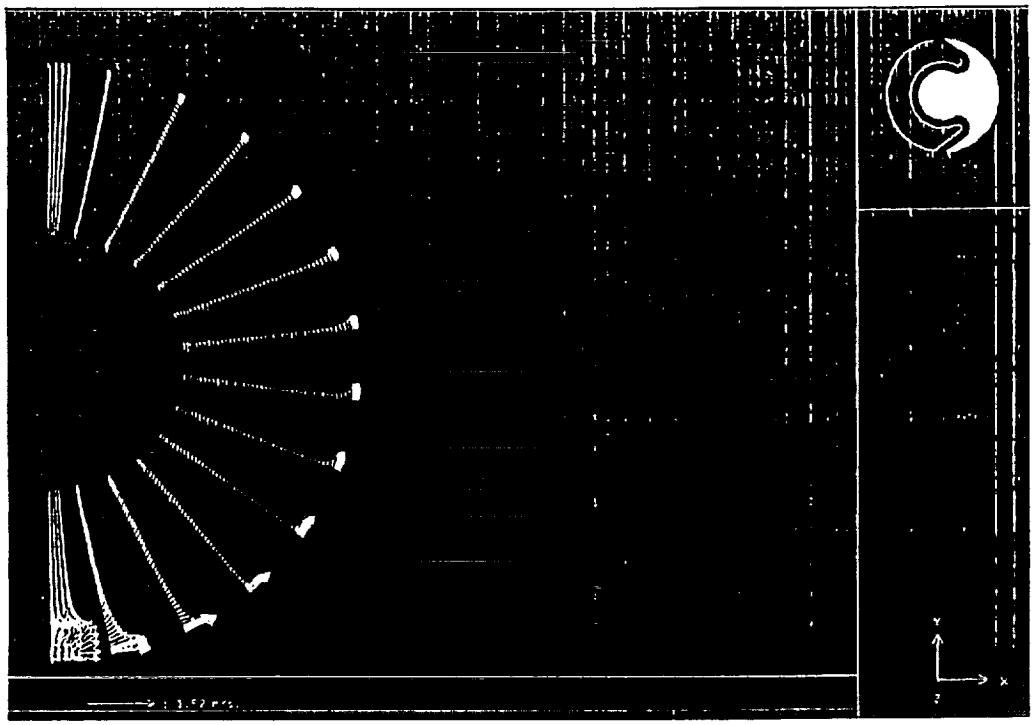

Figure 8: Velocity field on the axial direction symmetry plane

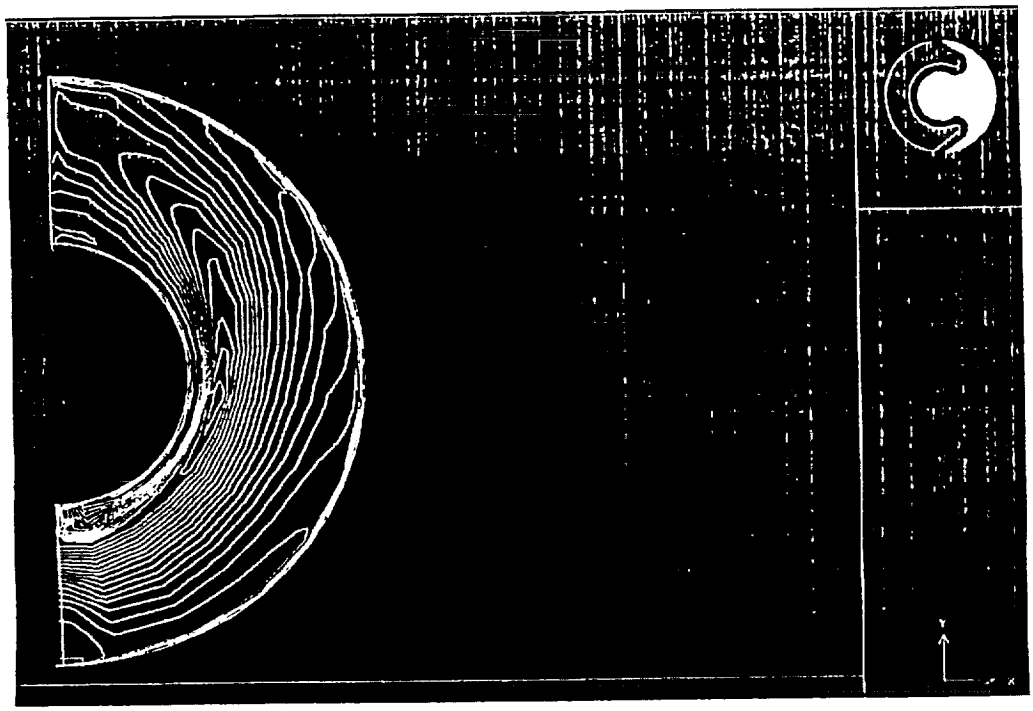

Figure 9: Coolant isotherms on the axial direction symmetry plane

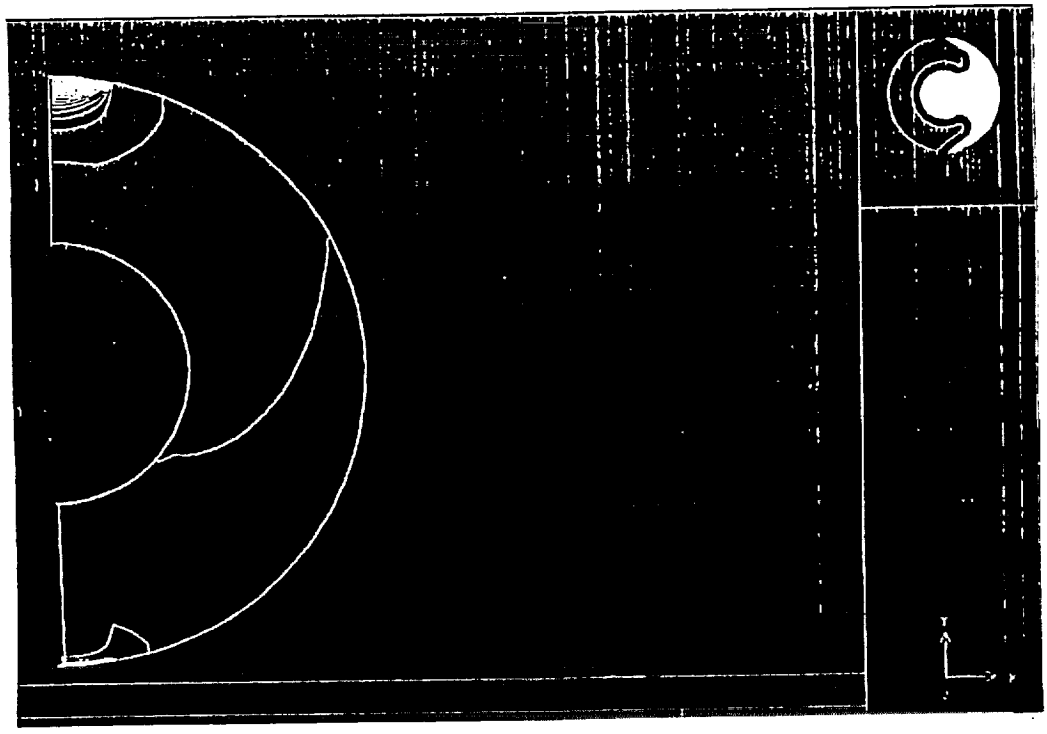

Figure 10: Isobars near the side wall of the housing

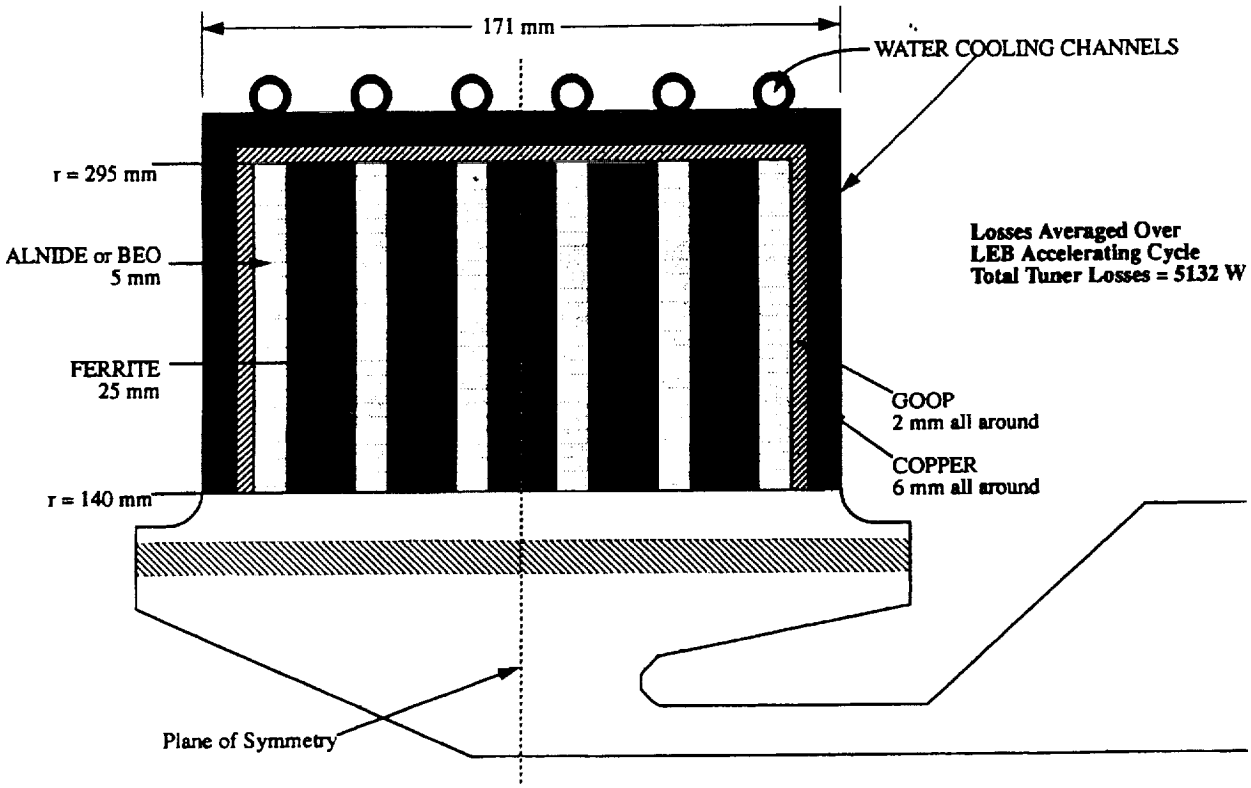

Figure 11: Sectional view of solid cooled low energy booster rf-cavity tuner

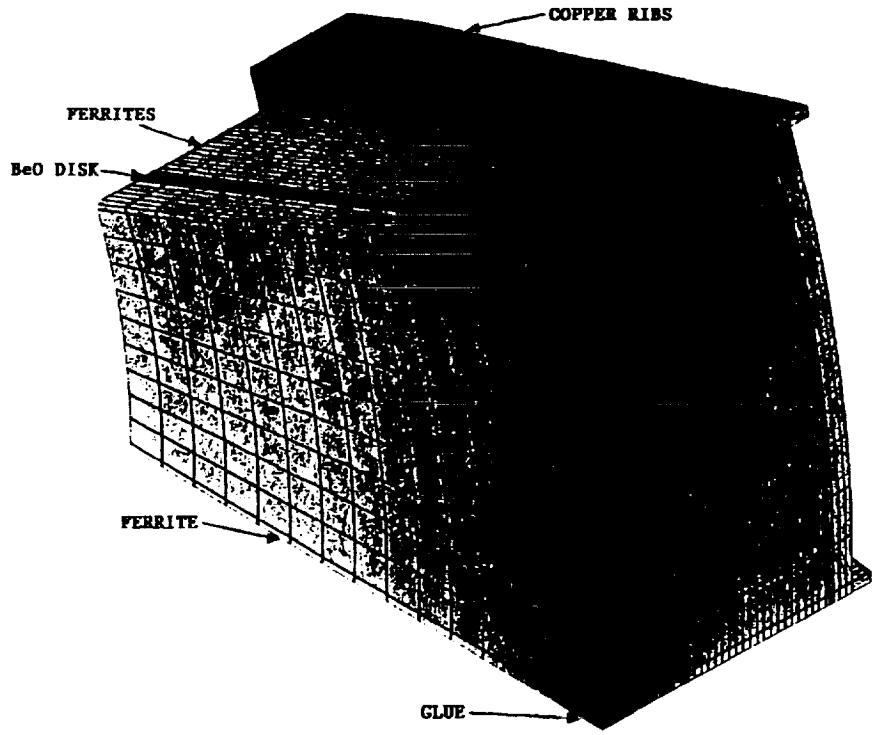

Figure 12a: Computational domain for the solid cooled low energy booster rf-cavity tuner - view 1

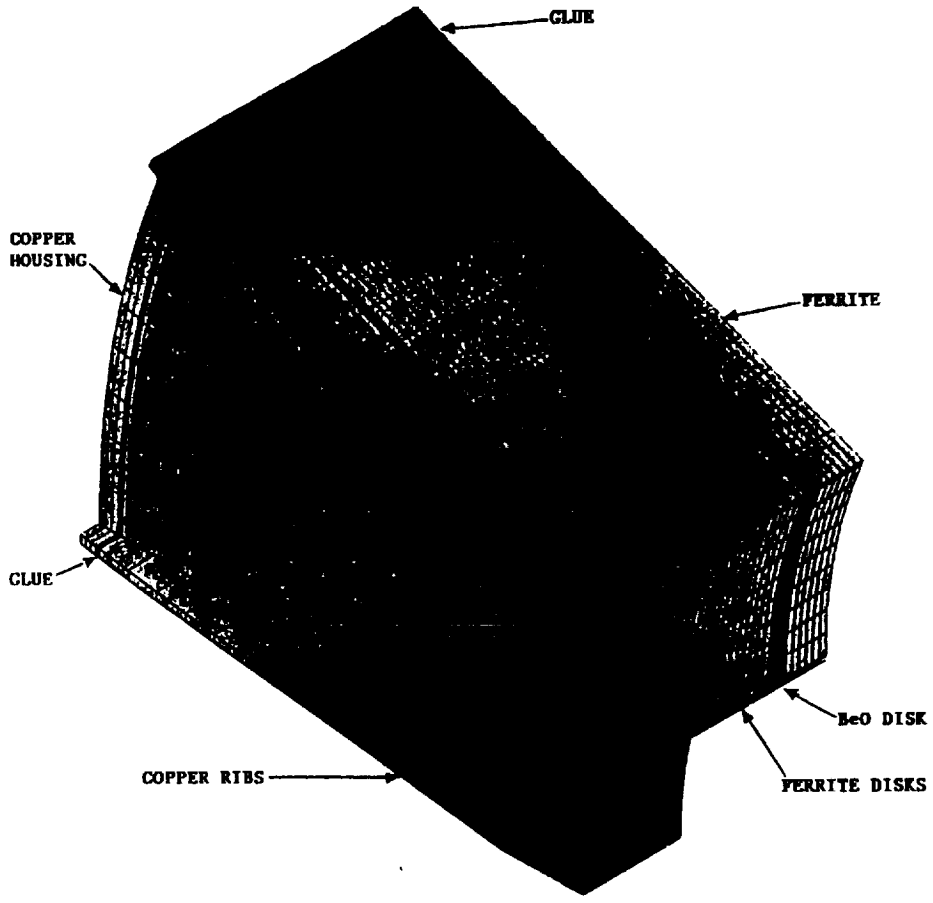

Figure 12b: Computational domain for the solid cooled low energy booster rf-cavity tuner - view 2